Measuring Complex Degree of Coherence of Random Light Fields with Generalized Hanbury Brown–Twiss Experiment

Zhaofeng Huang,[1] Yahong Chen,[1,*] Fei Wang,[1,†] Sergey A. Ponomarenko,[2,3] and Yangjian Cai[1,4,‡]

[1] *School of Physical Science and Technology and Collaborative Innovation Center of Suzhou Nano Science and Technology, Soochow University, Suzhou 215006, China*

[2] *Department of Electrical and Computer Engineering, Dalhousie University, Halifax, Nova Scotia B3J 2X4, Canada*

[3] *Department of Physics and Atmospheric Science, Dalhousie University, Halifax, Nova Scotia B3H 4R2, Canada*

[4] *Shandong Provincial Engineering and Technical Center of Light Manipulation and Shandong Provincial Key Laboratory of Optics and Photonic Device, School of Physics and Electronics, Shandong Normal University, Jinan 250014, China*

(Received 23 September 2019; revised manuscript received 4 March 2020; accepted 23 March 2020; published 15 April 2020)

We advance a protocol to measure the complex spatial degree of coherence of a partially coherent light field obeying Gaussian statistics through a generalized Hanbury Brown–Twiss (HBT) experiment. The proposed generalized HBT experiment amounts to combining a partially coherent field with a pair of coherent reference fields and measuring the intensity-intensity cross-correlation of the cumulative field. The real or imaginary part of the complex spatial degree of coherence can be extracted directly from the intensity-intensity cross-correlation by adjusting the phase delay between the two reference fields to be 0 or $\pi/2$. We test our method by carrying out a proof-of-principle experiment to measure the complex spatial degree of coherence of inhomogeneous light fields obeying Gaussian statistics. We find excellent agreement between the experimental results and our general theory. We show that our approach is extremely robust against the environmental fluctuations (e.g., the atmospheric turbulence) during the measurement. We demonstrate experimentally that a moving target hiding behind a ground-glass disk can be tracked with the aid of our complex-spatial-coherence measurement protocol.

DOI: 10.1103/PhysRevApplied.13.044042

I. INTRODUCTION

Coherence, as a fundamental resource in all areas of optical physics, from classical to quantum, plays a vital role in understanding interference, propagation, scattering, light-matter interactions, and other fundamental characteristics of both classical and quantum wave fields [1,2]. The magnitude of the second-order spatial degree of coherence of an optical field at a pair of points characterizes the strength of field correlations at the points. At the same time, the position-dependent phase of the degree of spatial coherence of a statistical source has been shown to be instrumental for generating partially coherent beams with adjustable far-zone angular distributions [3–5], propagation trajectories [6,7], and polarization patterns [7] in free space and linear media [8–10], as well as for engineering structured random solitons in noninstantaneous nonlinear media [11,12].

Thus, coherence measurements, especially those of the complex second-order spatial degree of coherence containing information about the second-order correlations among two or more spatial points within the statistical field, are significant from both the fundamental and applied perspectives. For instance, complex-spatial-coherence measurements play a crucial role in crystallography [13–15], quantitative phase imaging of biological tissues [16], the tracking of moving objects hidden from a scattering medium [17,18], and incoherent source reconstruction [19,20].

Various techniques have been proposed to measure the complex spatial coherence of statistical fields. The classical Young's interference experiment, among others, is the most common approach to measuring (two-point) complex spatial coherence. The amplitude and phase of the complex degree of coherence can be evaluated, respectively, from the visibility and the displacement of the interference fringes [1,14]. However, the methods based on Young's two-pinhole interferometry have several limitations. For example, the tiny size of the pinhole opening, necessary to maintain the spatial resolution of the complex

*yahongchen@suda.edu.cn
†fwang@suda.edu.cn
‡yangjiancai@suda.edu.cn

spatial degree of coherence [21], limits the light efficiency of the system; while acquiring the large sets of pinhole-separation data required for the full-field complex-coherence reconstruction [22], on the other hand, dramatically increases the measurement time. To overcome these limitations, other techniques have been developed, including wave-front-folding interferometry [23–27], coherence holography [28–32], and aperture (or obstacle) diffraction [33–35].

On the other hand, the classic Hanbury Brown–Twiss (HBT) experiment, involving higher-order correlation measurements (e.g., the intensity correlation) within the stochastic fields or among an ensemble of particles, has triggered the development of modern quantum optics, atomic physics, and astronomy [1]. According to the Siegert relation [1,36], an arbitrary high-order correlation among optical fields obeying Gaussian statistics can be expressed in terms of the second-order field correlations. However, only the modulus of the complex degree of coherence can be directly recovered by detecting the fluctuating intensity correlations [1,37–39]. Recently, it has been demonstrated that the real part of the complex degree of coherence of a statistical source can be experimentally reconstructed by performing a conventional HBT experiment with a strong coherent local oscillator [40]. However, the experimental protocol developed in Ref. [40] makes it possible to determine only the real part and the magnitude of the imaginary part of the complex degree of spatial coherence of a random source, thereby leaving the sign of the imaginary part and therefore the phase of the complex degree of spatial coherence indeterminate. Although the missing phase information can, in principle, be obtained by iterative phase-retrieval algorithms [15] or by a Hilbert-transform technique [36], these algorithms are prohibitively time-consuming in most situations of practical interest.

In this work, we propose a class of generalized HBT-type experiments *without any iterative phase-retrieval algorithm* to measure the complex spatial degree of coherence of optical fields obeying Gaussian statistics by introducing a pair of fully coherent reference fields. The real and imaginary parts—and hence the amplitude and phase—of the complex degree of coherence can be inferred from the *intensity cross-correlation* of the fluctuating optical fields. The power of the advanced method is demonstrated by carrying out proof-of-principle measurements of the complex spatial degree of coherence of an inhomogeneous partially coherent beamlike optical field [41–44]. We stress here that our protocol enables us to fully characterize complex two-dimensional light fields as well as their complex-valued spatial degrees of coherence, as opposed to the classic HBT-type experiments capable of recovering only either the modulus or the real part of the complex degree of coherence [37–40]. Further, our protocol is extremely robust to the environmental fluctuations, such as the atmospheric turbulence, during the measurement. This robustness feature does not exist in other types of interferometry, such as the Young's and wave-front-folding methods, due to the inherent sensitivity of the cross-spectral density phase to the environmental fluctuations [45–47]. Finally, we demonstrate experimentally that the proposed complex-coherence measurement protocol can be used to track a moving target.

This work is organized as follows. In Sec. II, we present our general protocol. In Sec. III, we present our experimental results to demonstrate the complex degree of coherence recovery of a partially coherent beam that we generate in the laboratory. Next, we show the robustness of our protocol to the environmental fluctuations, modeled through air-temperature fluctuations, in Sec. IV and we demonstrate the application of our protocol to moving target tracking in Sec. V. We summarize our findings in Sec. VI.

II. THEORY

Consider a scalar statistically stationary partially coherent source that propagates closely along the z axis. The second-order statistical (coherence) properties of the source field can be characterized, in the space-frequency domain, by an electric cross-spectral density function, namely [1]

$$W(\mathbf{r}_1, \mathbf{r}_2) = \langle E^*(\mathbf{r}_1) E(\mathbf{r}_2) \rangle, \tag{1}$$

where $E(\mathbf{r})$ is a field realization at a point $\mathbf{r}$ and at (angular) frequency ω, whereas the asterisk and angle brackets denote complex conjugation and ensemble averaging, respectively. Hereafter, we omit the frequency ω to streamline the notation. The spatial degree of coherence of the partially coherent field is defined as [1]

$$\mu(\mathbf{r}_1, \mathbf{r}_2) = \frac{W(\mathbf{r}_1, \mathbf{r}_2)}{\sqrt{S(\mathbf{r}_1) S(\mathbf{r}_2)}}, \tag{2}$$

where $S(\mathbf{r}) = W(\mathbf{r}, \mathbf{r}) = \langle I(\mathbf{r}) \rangle$ is an ensemble average of the field intensity. Here, $I(\mathbf{r}) = |E(\mathbf{r})|^2$ represents the intensity of a field realization. The spatial degree of coherence $\mu(\mathbf{r}_1, \mathbf{r}_2)$ is a complex-valued quantity and its amplitude $0 \leq |\mu(\mathbf{r}_1, \mathbf{r}_2)| \leq 1$, with the upper and lower limits corresponding to full coherence and complete lack of coherence, respectively, whereas the intermediate values represent partial coherence. According to the Siegert relation [1], $|\mu(\mathbf{r}_1, \mathbf{r}_2)|$, of a partially coherent field obeying Gaussian statistics, can be deduced from the field intensity-intensity autocorrelation $G(\mathbf{r}_1, \mathbf{r}_2) = \langle I(\mathbf{r}_1) I(\mathbf{r}_2) \rangle$, i.e.,

$$|\mu(\mathbf{r}_1, \mathbf{r}_2)| = \sqrt{G(\mathbf{r}_1, \mathbf{r}_2)/[S(\mathbf{r}_1) S(\mathbf{r}_2)] - 1}. \tag{3}$$

However, one can see that all phase information is lost in a conventional HBT experiment.

Let us now consider a generalized HBT-type experiment. To this end, we introduce a couple of independent coherent reference fields, $E_r^{(1)}(\mathbf{r})$ and $E_r^{(2)}(\mathbf{r})$. The combinations of the measured and reference fields read

$$E_S^{(1)}(\mathbf{r}) = E(\mathbf{r}) + E_r^{(1)}(\mathbf{r}), \tag{4}$$

$$E_S^{(2)}(\mathbf{r}) = E(\mathbf{r}) + E_r^{(2)}(\mathbf{r}), \tag{5}$$

where $E_S^{(1)}(\mathbf{r})$ and $E_S^{(2)}(\mathbf{r})$ denote the two composite field realizations.

In contrast to the intensity-intensity autocorrelation in the conventional HBT experiment, we seek the cross-correlation of the two composite field intensities, defined as

$$G_S^{(1,2)}(\mathbf{r}_1, \mathbf{r}_2) = \langle I_S^{(1)}(\mathbf{r}_1) I_S^{(2)}(\mathbf{r}_2) \rangle, \tag{6}$$

where $I_S^{(1)}(\mathbf{r})$ and $I_S^{(2)}(\mathbf{r})$ are the random intensities of the first and the second composite fields, respectively. For a statistical field obeying Gaussian statistics, the intensity-intensity cross-correlation function $G_S^{(1,2)}(\mathbf{r}_1, \mathbf{r}_2)$ can be expressed as (see the Appendix for the derivation)

$$\begin{aligned} G_S^{(1,2)}(\mathbf{r}_1, \mathbf{r}_2) &= G_S^{(1,2)}(\mathbf{r}_1, \mathbf{r}_2, \Delta\phi), \\ &= S_S^{(1)}(\mathbf{r}_1) S_S^{(2)}(\mathbf{r}_2) + |W(\mathbf{r}_1, \mathbf{r}_2)|^2 \\ &\quad + 2\sqrt{S_r^{(1)}(\mathbf{r}_1) S_r^{(2)}(\mathbf{r}_2)}\,\mathrm{Re}[e^{i\Delta\phi} W(\mathbf{r}_1, \mathbf{r}_2)]. \end{aligned} \tag{7}$$

Here, $\Delta\phi$ denotes the phase difference between two reference fields, i.e., $\Delta\phi = \mathrm{Arg}[E_r^{(1)}(\mathbf{r}_1)] - \mathrm{Arg}[E_r^{(2)}(\mathbf{r}_2)]$, where Arg denotes the phase of a complex function. Further, we introduce an explicit dependence on $\Delta\phi$, $G_S^{(1,2)}(\mathbf{r}_1, \mathbf{r}_2, \Delta\phi)$; $S_S^{(\upsilon)}(\mathbf{r}) = S_r^{(\upsilon)}(\mathbf{r}) + S(\mathbf{r})$, $\upsilon \in \{1, 2\}$, $S_r^{(\upsilon)}(\mathbf{r})$ being the intensity of the υth reference field and Re denoting the real part of a complex function.

It follows at once from Eq. (7) that, in general, both the real and the imaginary parts of the cross-spectral density $W(\mathbf{r}_1, \mathbf{r}_2)$ and, by implication, of the complex spatial degree of coherence, enter the expression for the intensity-intensity cross-correlation function. The real and imaginary parts of the complex degree of coherence can then be deduced by varying the phase difference $\Delta\phi$. We further note that an additional (and non-negligible) background contribution, $S_S^{(1)}(\mathbf{r}_1) S_S^{(2)}(\mathbf{r}_2) + |W(\mathbf{r}_1, \mathbf{r}_2)|^2$, is present as well. The background can be removed by figuring out the following background intensity-intensity cross-correction

$$G_B^{(1,2)}(\mathbf{r}_1, \mathbf{r}_2) = \langle [S_r^{(1)}(\mathbf{r}_1) + I(\mathbf{r}_1)][S_r^{(2)}(\mathbf{r}_2) + I(\mathbf{r}_2)] \rangle. \tag{8}$$

Next, applying the moment theorem for a Gaussian random process [1,36], we obtain

$$G_B^{(1,2)}(\mathbf{r}_1, \mathbf{r}_2) = S_S^{(1)}(\mathbf{r}_1) S_S^{(2)}(\mathbf{r}_2) + |W(\mathbf{r}_1, \mathbf{r}_2)|^2. \tag{9}$$

It then follows from Eqs. (7) and (9) that

$$\begin{aligned} \Delta G^{(1,2)}(\mathbf{r}_1, \mathbf{r}_2, \Delta\phi) &= G_S^{(1,2)}(\mathbf{r}_1, \mathbf{r}_2, \Delta\phi) - G_B^{(1,2)}(\mathbf{r}_1, \mathbf{r}_2) \\ &= 2\sqrt{S_r^{(1)}(\mathbf{r}_1) S_r^{(2)}(\mathbf{r}_2)}\,\mathrm{Re}[e^{i\Delta\phi} W(\mathbf{r}_1, \mathbf{r}_2)]. \end{aligned} \tag{10}$$

By setting $\Delta\phi$ in Eq. (10) to be 0 and $\pi/2$, respectively, and rearranging the formulas, we finally arrive at

$$\mathrm{Re}[\mu(\mathbf{r}_1, \mathbf{r}_2)] = \frac{\Delta G^{(1,2)}(\mathbf{r}_1, \mathbf{r}_2, \Delta\phi = 0)}{2\sqrt{S_r^{(1)}(\mathbf{r}_1) S_r^{(2)}(\mathbf{r}_2) S(\mathbf{r}_1) S(\mathbf{r}_2)}}, \tag{11}$$

$$\mathrm{Im}[\mu(\mathbf{r}_1, \mathbf{r}_2)] = \frac{\Delta G^{(1,2)}(\mathbf{r}_1, \mathbf{r}_2, \Delta\phi = \frac{\pi}{2})}{2\sqrt{S_r^{(1)}(\mathbf{r}_1) S_r^{(2)}(\mathbf{r}_2) S(\mathbf{r}_1) S(\mathbf{r}_2)}}, \tag{12}$$

where Im denotes the imaginary part of a complex function.

Equations (11) and (12) clearly imply that when we introduce a pair of coherent reference fields with phase difference $\Delta\phi = 0$ or $\pi/2$ into a HBT-type experiment, the complex (real and imaginary parts of) spatial degree of coherence of a partially coherent light field can be recovered from the intensity-intensity cross-correlation of the superposed statistical fields. This is the key result of this paper.

We note that the spatial resolution of the measured spatial degree of coherence is merely determined by the field-intensity detector. For example, by using a commercial charge-coupled device (CCD) for detecting the intensities, we can resolve spatial-coherence features with a spatial resolution of approximately 4 μm. In addition, unlike Young's two-pinhole experiment [21], our approach does not need any diffracting apertures or obstacles, thereby avoiding any light-efficiency loss in the system. For statistically stationary fields, the ensemble average is equivalent to the time average [2,36]. Thus, the fast response rate of a CCD ensures the fast measurement of the complex degree of coherence. Furthermore, in some cases, such as for the partially coherent light fields generated by the Fourier or Fresnel transformation optical systems, the ensemble average can be replaced with the spatial average of a speckle field [32], implying that in such cases, the spatial degree of coherence can be recovered virtually in real time.

III. EXPERIMENT

We now carry out a proof-of-principle experiment to measure the complex spatial coherence of a scalar partially coherent light beam [42–44]. In our experiment, the orthogonal components of a right-handed circularly polarized beam are used as a pair of coherent reference fields with a stable $\pi/2$ phase difference. A combined field of

the $\pi/4$-linearly polarized partially coherent beam and a right-handed circularly polarized beam can be written as

$$\begin{aligned}\mathbf{E}_S(\mathbf{r}) &= E_S^{(x)}\hat{\mathbf{e}}_x + E_S^{(y)}\hat{\mathbf{e}}_y \\ &= [E(\mathbf{r}) + E_x^{\mathrm{RCP}}(\mathbf{r})]\hat{\mathbf{e}}_x + [E(\mathbf{r}) + E_y^{\mathrm{RCP}}(\mathbf{r})]\hat{\mathbf{e}}_y, \quad (13)\end{aligned}$$

where $E(\mathbf{r})$ is a field realization of the partially coherent beam and $E_x^{\mathrm{RCP}}(\mathbf{r})$ and $E_y^{\mathrm{RCP}}(\mathbf{r})$ are the x and y components of the right-handed circularly polarized reference beam, respectively, whereas $\hat{\mathbf{e}}_x$ and $\hat{\mathbf{e}}_y$ are the Cartesian unit vectors in the x and y directions. Here, $\mathrm{Arg}[E_x^{\mathrm{RCP}}(\mathbf{r})] - \mathrm{Arg}[E_y^{\mathrm{RCP}}(\mathbf{r})] = \pi/2$. Thus, by simultaneously measuring the random intensities of the x and y components of the combined field with two CCDs, we can recover the real and imaginary parts of the complex degree of coherence of the partially coherent beam following our protocol.

Figure 1 shows our experimental setup. An x-polarized beam, created by transmitting a He-Ne laser of wavelength 633 nm through a linear polarizer (LP), is split by a beam splitter (BS) into two beams that go into the top and bottom arms shown in Fig. 1, respectively. The purpose of the bottom arm is to generate a partially coherent light beam with prescribed coherence properties, while the top arm is used to create a coherent circularly polarized reference beam. In the bottom arm, a linearly polarized beam, having passed through a neutral-density filter (NDF) and been expanded by a beam expander (BE) to generate a collimated output, is impinged onto a spatial light modulator (SLM) for generating a coherent light beam with an adjustable intensity profile [say, $p(\mathbf{v})$, where $\mathbf{v}$ denotes a radius vector in the SLM plane]. The SLM-shaped coherent beam is then projected onto a rotating ground-glass disk (RGGD) by a $2f$ imaging system formed by a thin lens L_1 of focal distance $f_1 = 150$ mm, producing a spatially incoherent beam of intensity $p(\mathbf{v})$ with its cross-spectral density given by the expression

$$W(\mathbf{v}_1, \mathbf{v}_2) = p(\mathbf{v}_1)\delta(\mathbf{v}_1 - \mathbf{v}_2). \quad (14)$$

Here, $\delta(\mathbf{v}_1 - \mathbf{v}_2)$ is a Dirac delta function. We stress that the beam transmitted by a RGGD can be regarded as an incoherent secondary source if the beam spot size on the RGGD is much larger than a characteristic inhomogeneity scale of the RGGD [36]—a condition that is well satisfied in our experiment. As the emerging incoherent secondary source has been shaped by a Fourier-transforming system, a thin lens L_2 of focal length $f_2 = 250$ mm, the spatial degree of coherence of the resulting Fourier-transformed beam can be expressed as [41]

$$\mu(\mathbf{r}_1, \mathbf{r}_2) = \frac{1}{\lambda^2 f_2^2}\int d^2\mathbf{v} p(\mathbf{v}) \exp\left[\frac{i2\pi}{\lambda f_2}(\mathbf{r}_1 - \mathbf{r}_2)\cdot\mathbf{v}\right], \quad (15)$$

where λ is the wavelength of light. We note that the partially coherent beam generated in this manner is of a Schell-model type, with a statistically homogeneous spatial degree of coherence $\mu(\mathbf{r}_1, \mathbf{r}_2) = \mu(\mathbf{r}_1 - \mathbf{r}_2)$. Further, the generated partially coherent beam obeys Gaussian statistics, since it is generated by an incoherent source from a RGGD [36]. We note that since the partially coherent beam in our case is generated by a Fourier-transforming optical system, the ensemble average in the data processing

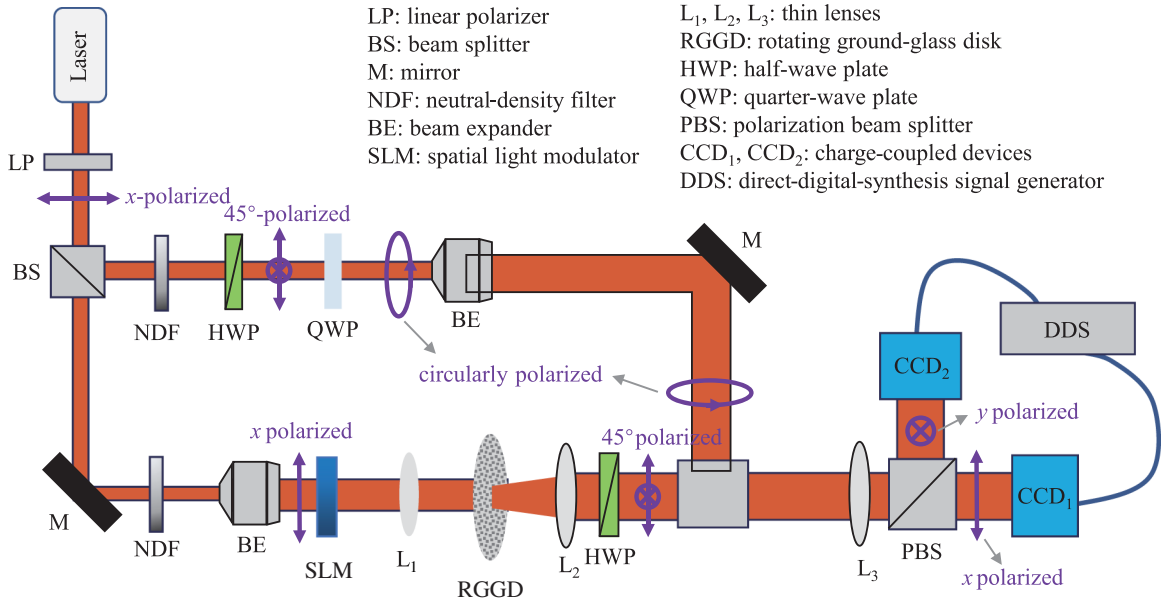

FIG. 1. The schematic of the experimental setup for the complex-spatial-coherence measurement of a partially coherent beam with the inhomogeneous coherence feature.The purple arrows denote the polarization direction of the light beam.

can be replaced with the spatial average [32]. The generated scalar partially coherent beam then passes through a half-wave plate (HWP), with its fast axis making an angle $\pi/8$ with respect to the x-polarization direction, to yield a partially coherent beam that is linearly polarized at the angle $\pi/4$ to the x-polarization direction.

In the top reference arm of Fig. 1, the linearly polarized beam is transmitted through the NDF, the HWP, and a quarter-wave plate (QWP). The fast axis of the HWP is set to be $\pi/8$ with respect to the x-polarization direction, while the fast axis of the QWP is set to be parallel to the x-polarization direction. Therefore, a right-handed circularly polarized beam is generated immediately after the QWP. The circularly polarized reference beam is then expanded by the beam expander, producing a beam of virtually uniform intensity. Due to the $\pi/2$ phase difference between the two orthogonal components of the circularly polarized beam, its x and y components can be viewed as a pair of reference fields required for our protocol. We display the experimentally measured intensity distributions of the x and y components $S_x^{\mathrm{RCP}}(\mathbf{r})$ and $S_y^{\mathrm{RCP}}(\mathbf{r})$ of the reference field in Figs. 2(a) and 2(b), respectively.

Next, we combine the circularly polarized reference field and the generated $\pi/4$-linearly polarized partially coherent beam at the BS. The x- and y-component fields of the composite field are then split by a polarization beam splitter (PBS) and imaged, respectively, onto CCD_1 and CCD_2 by a $2f$ imaging system formed by a couple of thin lenses L_3 of focal distance $f_3 = 250$ mm. A direct-digital-synthesis (DDS) signal generator is used as an external trigger for controlling the two CCDs, to simultaneously capture the intensities of the x- and y-component fields of the composite random field, $I_S^{(1)}(\mathbf{r})$ and $I_S^{(2)}(\mathbf{r})$.

In our experiment, an off-axis circular ring is loaded onto the intensity-modulating SLM. We show the intensity distribution $p(\mathbf{v})$ of the circular ring, illuminating the RGGD, in Fig. 2(c). The internal and external diameters of the circular ring are 2.40 mm and 3.43 mm, respectively. The displacement of the ring center is $|\mathbf{v}_0| = 0.97$ mm with respect to the optical axis. Such a spatial displacement of $p(\mathbf{v})$ in Eq. (15) will lead to a phase shift in the degree of coherence $\mu(\mathbf{r}_1, \mathbf{r}_2)$ [6,7], ensuring the nonzero imaginary part of $\mu(\mathbf{r}_1, \mathbf{r}_2)$. Once the distribution of $p(\mathbf{v})$ is known, we can calculate $\mu(\mathbf{r}_1, \mathbf{r}_2)$ by using Eq. (15), where $\mu(\mathbf{r}_1, \mathbf{r}_2)$ and $p(\mathbf{v})$ form a Fourier-transformation pair. The top panels of Fig. 3 illustrate the numerical calculations of the real $\mu'(\Delta\mathbf{r})$ and imaginary $\mu''(\Delta\mathbf{r})$ parts and the square modulus $|\mu(\Delta\mathbf{r})|^2$ of the spatial complex degree of coherence of the generated partially coherent beam, where prime and double prime denote the real and imaginary parts, respectively, and $\Delta\mathbf{r} = \mathbf{r}_1 - \mathbf{r}_2$. We compare these theoretical results with the experimental results later.

To measure $\mu(\mathbf{r}_1, \mathbf{r}_2)$ experimentally, we further need to know the intensity distributions $I(\mathbf{r})$ of the partially coherent field and $I_S^{(1)}(\mathbf{r})$, as well as $I_S^{(2)}(\mathbf{r})$, of the two

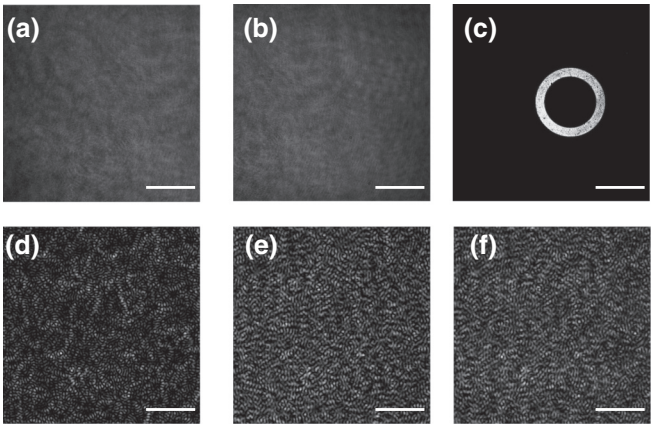

FIG. 2. The experimental results for the intensity distributions: (a) $S_x^{\mathrm{RCP}}(\mathbf{r})$, the x component of the circularly polarized reference field; (b) $S_y^{\mathrm{RCP}}(\mathbf{r})$, the y component of the circularly polarized reference field; (c) $p(\mathbf{v})$, the controlled-shape beam projected onto the RGGD; (d) $I(\mathbf{r})$, the generated partially coherent beam; (e) $I_S^{(1)}(\mathbf{r})$; and (f) $I_S^{(2)}(\mathbf{r})$, two composite statistical fields. The scale bars in (a), (b), (d), (e), and (f) are 1.32 mm, while the scale bar in (c) is 2.25 mm.

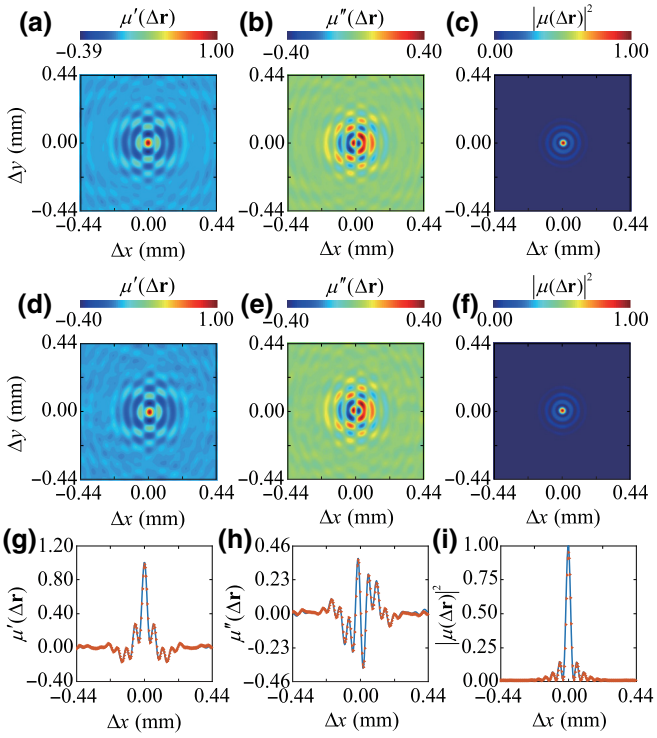

FIG. 3. (a)–(c) Simulation and (d)–(f) experimental results for the real $\mu'(\Delta\mathbf{r})$ and imaginary $\mu''(\Delta\mathbf{r})$ parts and the square modulus $|\mu(\Delta\mathbf{r})|^2$ of the complex spatial degree of coherence of the generated partially coherent light beam. (g)–(i) The cross line ($\Delta y = 0$) of the simulation (blue solid curves) and the experimental results (red triangles).

composite statistical fields. We exhibit the experimental results for the intensity distributions in Figs. 2(d)–2(f). The intensity-intensity correlation in Eq. (10) can thus be obtained as

$$G_S^{(1,2)}(\mathbf{r}_1,\mathbf{r}_2,\Delta\phi=0)=\langle I_S^{(1)}(\mathbf{r}_1)I_S^{(1)}(\mathbf{r}_2)\rangle_s, \tag{16}$$

$$G_S^{(1,2)}(\mathbf{r}_1,\mathbf{r}_2,\Delta\phi=\frac{\pi}{2})=\langle I_S^{(1)}(\mathbf{r}_1)I_S^{(2)}(\mathbf{r}_2)\rangle_s, \tag{17}$$

$$G_B^{(1,2)}(\mathbf{r}_1,\mathbf{r}_2)=\langle[S_x^{\mathrm{RCP}}(\mathbf{r}_1)+I(\mathbf{r}_1)]\times[S_y^{\mathrm{RCP}}(\mathbf{r}_2)+I(\mathbf{r}_2)]\rangle_s, \tag{18}$$

where $\langle\cdot\rangle_s$ denotes spatial averaging. Here, $G_S^{(1,2)}(\mathbf{r}_1,\ \mathbf{r}_2,\ \Delta\phi=0)$ can also be obtained by $\langle I_S^{(2)}(\mathbf{r}_1)I_S^{(2)}(\mathbf{r}_2)\rangle_s$. We further substitute for the intensity-intensity correlation functions from Eqs. (16)–(18) into Eqs. (10)–(12) to recover the real and imaginary parts of the complex spatial degree of coherence. In the middle panel row of Fig. 3, we show the experimental results for the real and imaginary parts of $\mu(\Delta\mathbf{r})$ of the generated partially coherent beam. The square modulus of the spatial degree of coherence follows from $|\mu'(\Delta\mathbf{r})|^2+|\mu''(\Delta\mathbf{r})|^2$. In the bottom panel row of Fig. 3, we show the cross line ($\Delta y=0$) of the simulation and the experimental results for the degree of coherence. Comparing our experimental and theoretical results, we find that our experimental results are very consistent with the advanced theory. In our experiment, the spatial resolution of the measured degree of coherence is solely determined by the spatial resolution of the CCD, which is 4.4 μm $\times$ 4.4 μm, implying the same spatial resolution for the complex degree of coherence.

IV. ROBUSTNESS OF THE MEASUREMENT

Next, we examine the robustness of our protocol by introducing environmental fluctuations during the measurement. To this end, we let the composite statistical field, consisting of the partially coherent source and the reference light, pass through a thermally induced turbulence, generated by a hot graphitic plate with a controllable temperature-T distribution. The turbulence strength increases with the plate temperature T [48]. To show the

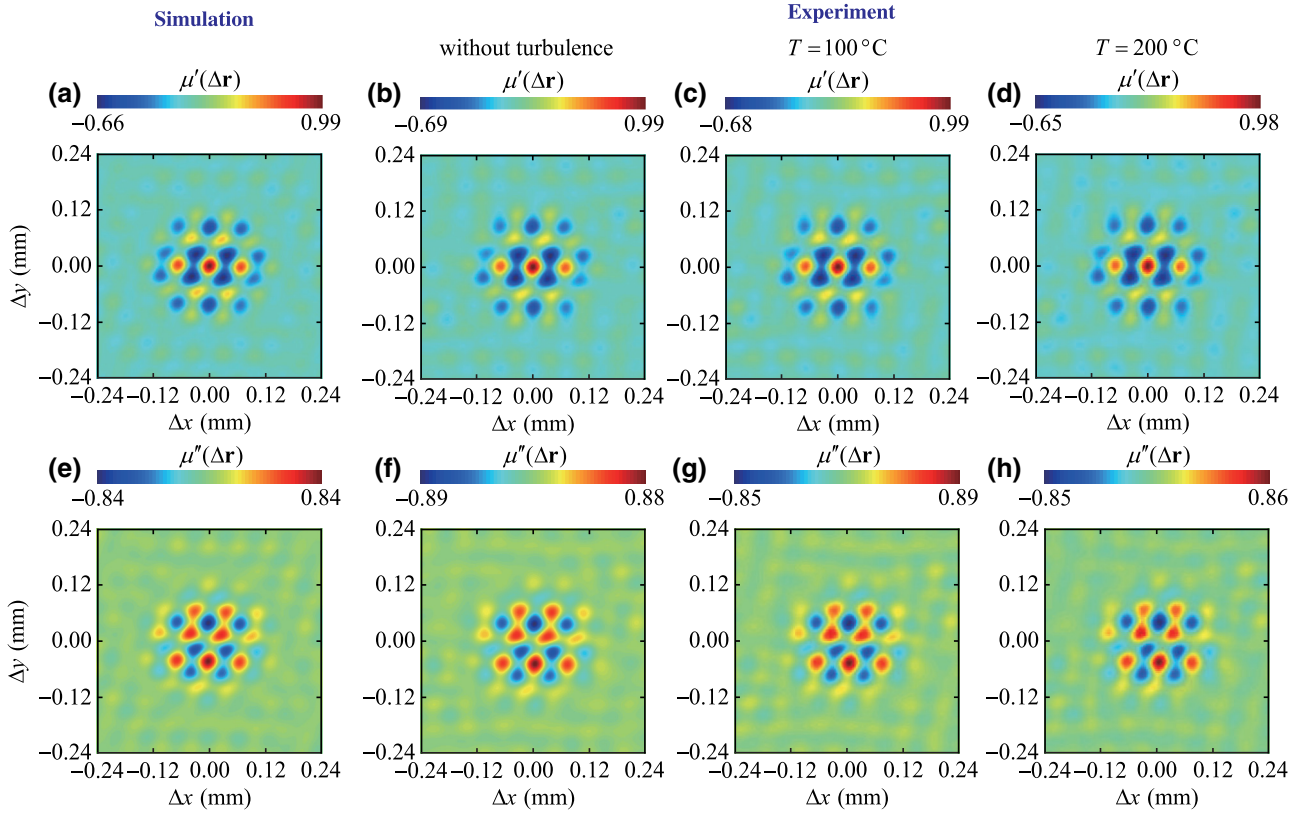

FIG. 4. The robustness of the complex degree of coherence measurement in the face of thermally induced turbulence modeling of the atmospheric turbulence. (a),(e) Simulation results for the real $\mu'(\Delta\mathbf{r})$ and imaginary $\mu''(\Delta\mathbf{r})$ parts of the complex spatial degree of coherence of the generated partially coherent light. Experimental results for $\mu'(\Delta\mathbf{r})$ and $\mu''(\Delta\mathbf{r})$ measured [(b),(f)] without turbulence and [(c),(g); (d),(h)] in the presence of thermally induced turbulence, with the temperature T of the hot graphitic plate being 100 °C and 200 °C, respectively.

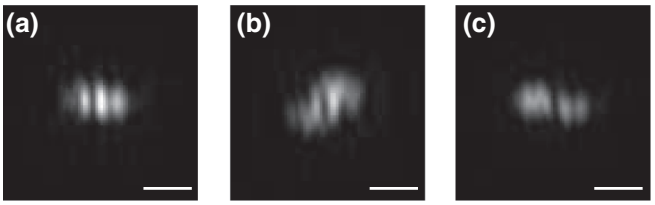

FIG. 5. The experimental results for the Young's interference pattern (one realization) with the generated partially coherent source at the focal plane: (a) no turbulence present; (b),(c) turbulence induced by the hot graphitic plate of temperature $T =$ 100 °C and 200 °C, respectively. The focal distance of the focal lens is 150 mm. The scale bars in (a)–(c) are 40 μm.

versatility of our experiment, we replace the circular ring loaded by the SLM of Fig. 1 with three opening circular pinholes of diameter 1.5 mm each. Connecting the centers of the three pinholes, one can form an equilateral triangle of the side 5.6 mm. The displacement position of the triangle center with respect to the optical axis is given by the radius vector $\mathbf{v}_0 = (0, -1)$ mm. In Figs. 4(a) and 4(e), we display the simulation results for the real and imaginary parts of the complex spatial degree of coherence of the partially coherent source with the given distribution of $p(\mathbf{v})$. In Figs. 4(b) and 4(f), we show the panels corresponding to the experimental results obtained without turbulence. The experimental results, shown in Figs. 4(b) and 4(f), are consistent with the simulations. When we heat the graphitic plate, the air density in the measurement path varies rapidly, thereby causing variations in the index of refraction (thermally induced turbulence). Under such induced turbulence, the optical field fluctuates at random and the field-intensity distribution is distorted. For example, see Fig. 5, where we display a (focused) interference pattern,

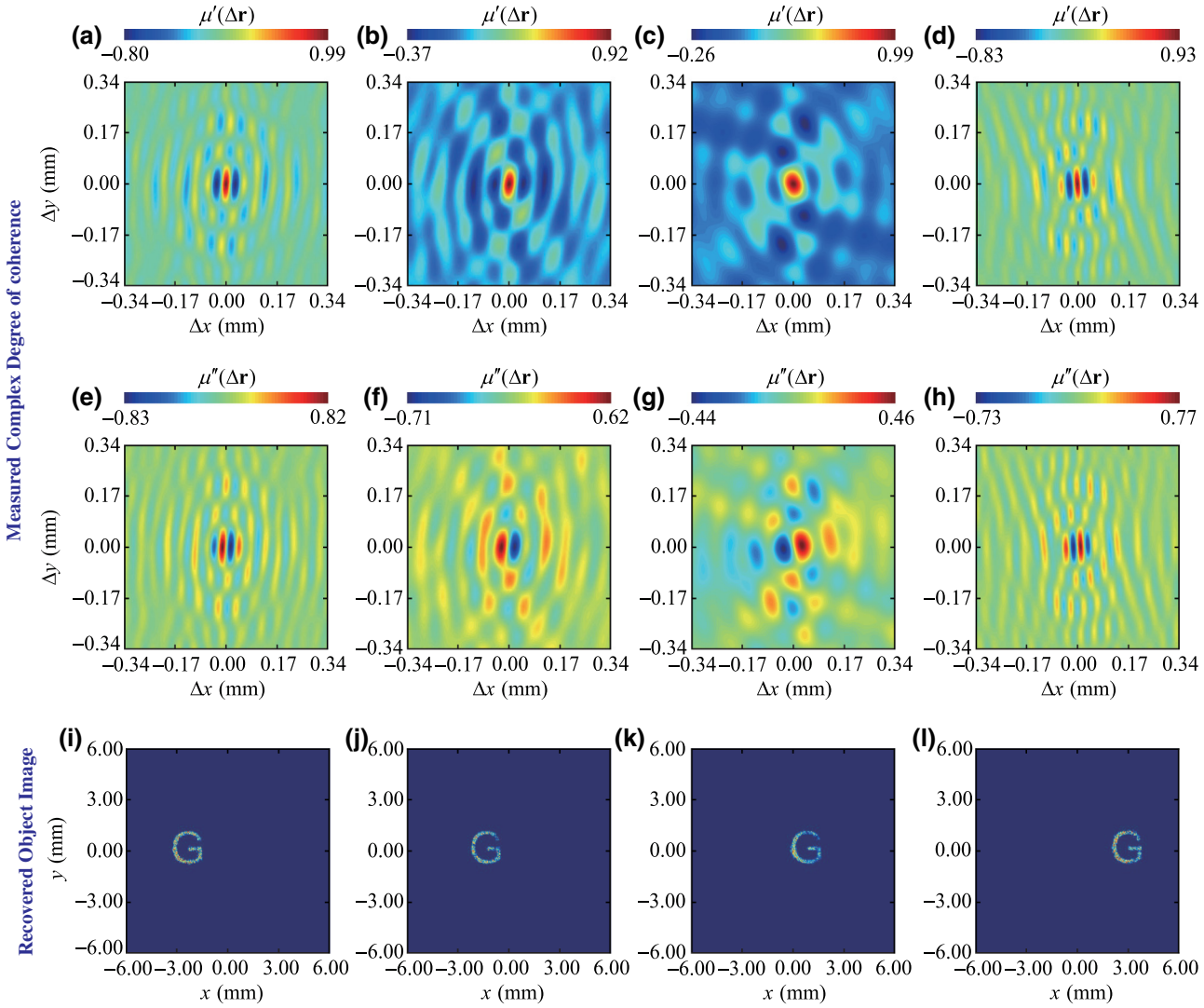

FIG. 6. Tracking a moving object (a moving letter "G") hiding behind the RGGD in the experimental setup of Fig. 1. (a)–(h) The measured complex (real and imaginary parts) of the spatial degree of coherence of the random light associated with the moving object at different transverse positions. (i)–(l) The corresponding recovered-object images from the measured complex degrees of coherence.

generated by a partially coherent source, which is transmitted through a Young's two-pinhole interferometer and the thermally induced turbulence of a controlled temperature distribution. We can see in the figure that whenever the turbulence is present, the fringes are distorted, reducing the interference-fringe visibility and implying that the source spatial degree of coherence can never be recovered. At the same time, the (complex) spatial degree of coherence in the presence of turbulence, measured by our protocol, is effectively free from turbulence-induced degradation, as is evidenced in Figs. 4(c), 4(g), 4(d), and 4(h). These results indicate the extreme robustness of our measurement against environmental fluctuations. We further stress that although we only consider the quasimonochromatic case, our protocol can show the dispersion-cancelation effect for polychromatic situations [49–51]. As a result, our approach can be useful for imaging and position tracking of moving targets through complex random media.

V. APPLICATION TO MOVING TARGET TRACKING

We now show that our complex-spatial-coherence measurement protocol is capable of tracking both the position and shape of a moving object hidden behind the ground-glass disk. The main principle is encapsulated in Eq. (15), revealing that the spatial degree of coherence $\mu(\mathbf{r}_1, \mathbf{r}_2)$ and the intensity profile $p(\mathbf{v})$ of the object behind the ground-glass disk form a Fourier-transformation pair. Thus, once the complex spatial degree of coherence $\mu(\mathbf{r}_1, \mathbf{r}_2)$ is determined following our protocol, the intensity profile of the moving object, including its position and shape, can be recovered. We demonstrate this application using our experimental setup shown in Fig. 1. The moving object, located behind the RGGD and generated by the SLM, is a letter "G" moving along a straight line. The first two top panels of Fig. 6 display the experimental results of the real and imaginary parts of the complex spatial degree of coherence of the random fields associated with the moving letter "G" at several positions in a transverse plane. The bottom panel of Fig. 6 shows the corresponding object images of the letter "G" at different positions recovered from the measured complex spatial coherence. The experiment confirms that both the shape and position of the object image hiding behind the ground-glass disk can be tracked well via the proposed protocol. In addition, we carry out the tracking application in the presence of laboratory-generated thermal turbulence, as shown in Sec. IV. The experiment (not shown here) reveals that the recovered object image is effectively free of the turbulence fluctuations.

VI. CONCLUSIONS

We demonstrate both theoretically and experimentally that the complex spatial degree of coherence of a partially coherent light field obeying Gaussian statistics can be efficiently measured by introducing a pair of reference coherent fields within the framework of a classic HBT type experiment. Our results show that the proposed spatial-coherence measurement protocol based on the intensity-intensity cross-correlation is extremely robust against environmental fluctuations during the measurement. As most natural sources obey Gaussian statistics, our protocol is pertinent to a wide class of light sources, encountered in nature or simulated in the laboratory. We further demonstrate experimentally that the measured complex (amplitude and phase) information of the spatial degree of coherence, which can never be detected by the conventional HBT experiment, can find applications in the tracking of a moving target concealed within a scattering medium.

ACKNOWLEDGMENTS

This work was supported by the National Key Research and Development Project of China (Grant No. 2019YFA0705000), the National Natural Science Foundation of China (NSFC) (Grants No. 11525418, 91750201, 11874046, 11974218, and 11904247), the Innovation Group of Jinan (Grant No. 2018GXRC010), the Natural Sciences and Engineering Research Council of Canada (Grant No. RGPIN-2018-05497), the Natural Science Foundation of the Jiangsu Higher Education Institutions of China (Grant No. 19KJB140017), the China Postdoctoral Science Foundation (Grant No. 2019M661915), the Natural Science Foundation of Shandong Province (Grant No. ZR2019QA004), the Priority Academic Program Development of Jiangsu Higher Education Institutions, and the Qing Lan Project of Jiangsu Province of China.

APPENDIX: DERIVATION OF EQ. (7)

To derive the intensity-intensity cross-correlation function $G_S^{(1,2)}(\mathbf{r}_1, \mathbf{r}_2)$ of the two composite field intensities, we first write out the intensities in an explicit form as

$$I_S^{(1)}(\mathbf{r}) = S_r^{(1)}(\mathbf{r}) + I(\mathbf{r}) + E_r^{(1)*}(\mathbf{r})E(\mathbf{r}) + E_r^{(1)}(\mathbf{r})E^*(\mathbf{r}), \tag{A1}$$

$$I_S^{(2)}(\mathbf{r}) = S_r^{(2)}(\mathbf{r}) + I(\mathbf{r}) + E_r^{(2)*}(\mathbf{r})E(\mathbf{r}) + E_r^{(2)}(\mathbf{r})E^*(\mathbf{r}). \tag{A2}$$

Substituting from Eqs. (A1) and (A2) into Eq. (6), we obtain that $G_S^{(1,2)}(\mathbf{r}_1, \mathbf{r}_2)$ can be expressed as a sum of 16 terms, as follows:

$$G_{S,1}^{(1,2)}(\mathbf{r}_1, \mathbf{r}_2) = S_r^{(1)}(\mathbf{r}_1)S_r^{(2)}(\mathbf{r}_2), \tag{A3}$$

$$G_{S,2}^{(1,2)}(\mathbf{r}_1, \mathbf{r}_2) = S_r^{(1)}(\mathbf{r}_1)\langle I(\mathbf{r}_2)\rangle, \tag{A4}$$

$$G_{S,3}^{(1,2)}(\mathbf{r}_1, \mathbf{r}_2) = S_r^{(1)}(\mathbf{r}_1)E_r^{(2)*}(\mathbf{r}_2)\langle E(\mathbf{r}_2)\rangle, \tag{A5}$$

$$G_{S,4}^{(1,2)}(\mathbf{r}_1,\mathbf{r}_2) = S_r^{(1)}(\mathbf{r}_1)E_r^{(2)}(\mathbf{r}_2)\langle E^*(\mathbf{r}_2)\rangle, \tag{A6}$$

$$G_{S,5}^{(1,2)}(\mathbf{r}_1,\mathbf{r}_2) = \langle I(\mathbf{r}_1)\rangle S_r^{(2)}(\mathbf{r}_2), \tag{A7}$$

$$G_{S,6}^{(1,2)}(\mathbf{r}_1,\mathbf{r}_2) = \langle I(\mathbf{r}_1)I(\mathbf{r}_2)\rangle, \tag{A8}$$

$$G_{S,7}^{(1,2)}(\mathbf{r}_1,\mathbf{r}_2) = \langle I(\mathbf{r}_1)E(\mathbf{r}_2)\rangle E_r^{(2)*}(\mathbf{r}_2), \tag{A9}$$

$$G_{S,8}^{(1,2)}(\mathbf{r}_1,\mathbf{r}_2) = \langle I(\mathbf{r}_1)E^*(\mathbf{r}_2)\rangle E_r^{(2)}(\mathbf{r}_2), \tag{A10}$$

$$G_{S,9}^{(1,2)}(\mathbf{r}_1,\mathbf{r}_2) = E_r^{(1)*}(\mathbf{r}_1)\langle E(\mathbf{r}_1)\rangle S_r^{(2)}(\mathbf{r}_2), \tag{A11}$$

$$G_{S,10}^{(1,2)}(\mathbf{r}_1,\mathbf{r}_2) = E_r^{(1)*}(\mathbf{r}_1)\langle E(\mathbf{r}_1)I(\mathbf{r}_2)\rangle, \tag{A12}$$

$$G_{S,11}^{(1,2)}(\mathbf{r}_1,\mathbf{r}_2) = E_r^{(1)*}(\mathbf{r}_1)\langle E(\mathbf{r}_1)E(\mathbf{r}_2)\rangle E_r^{(2)*}(\mathbf{r}_2), \tag{A13}$$

$$G_{S,12}^{(1,2)}(\mathbf{r}_1,\mathbf{r}_2) = E_r^{(1)*}(\mathbf{r}_1)\langle E(\mathbf{r}_1)E^*(\mathbf{r}_2)\rangle E_r^{(2)}(\mathbf{r}_2), \tag{A14}$$

$$G_{S,13}^{(1,2)}(\mathbf{r}_1,\mathbf{r}_2) = E_r^{(1)}(\mathbf{r}_1)\langle E^*(\mathbf{r}_1)\rangle S_r^{(2)}(\mathbf{r}_2), \tag{A15}$$

$$G_{S,14}^{(1,2)}(\mathbf{r}_1,\mathbf{r}_2) = E_r^{(1)}(\mathbf{r}_1)\langle E^*(\mathbf{r}_1)I(\mathbf{r}_2)\rangle, \tag{A16}$$

$$G_{S,15}^{(1,2)}(\mathbf{r}_1,\mathbf{r}_2) = E_r^{(1)}(\mathbf{r}_1)\langle E^*(\mathbf{r}_1)E(\mathbf{r}_2)\rangle E_r^{(2)*}(\mathbf{r}_2), \tag{A17}$$

$$G_{S,16}^{(1,2)}(\mathbf{r}_1,\mathbf{r}_2) = E_r^{(1)}(\mathbf{r}_1)\langle E^*(\mathbf{r}_1)E^*(\mathbf{r}_2)\rangle E_r^{(2)}(\mathbf{r}_2). \tag{A18}$$

It follows from the moment theorem for a Gaussian random process that ten of the above 16 terms vanish, i.e., $G_{S,3}^{(1,2)}(\mathbf{r}_1,\mathbf{r}_2)$, $G_{S,4}^{(1,2)}(\mathbf{r}_1,\mathbf{r}_2)$, $G_{S,7}^{(1,2)}(\mathbf{r}_1,\mathbf{r}_2)$, $G_{S,8}^{(1,2)}(\mathbf{r}_1,\mathbf{r}_2)$, $G_{S,9}^{(1,2)}(\mathbf{r}_1,\mathbf{r}_2)$, $G_{S,10}^{(1,2)}(\mathbf{r}_1,\mathbf{r}_2)$, $G_{S,11}^{(1,2)}(\mathbf{r}_1,\mathbf{r}_2)$, $G_{S,13}^{(1,2)}(\mathbf{r}_1,\mathbf{r}_2)$, $G_{S,14}^{(1,2)}(\mathbf{r}_1,\mathbf{r}_2)$, and $G_{S,16}^{(1,2)}(\mathbf{r}_1,\mathbf{r}_2) = 0$. In addition, we have the following:

$$\langle I(\mathbf{r})\rangle = S(\mathbf{r}), \tag{A19}$$

$$\langle I(\mathbf{r}_1)I(\mathbf{r}_2)\rangle = S(\mathbf{r}_1)S(\mathbf{r}_2) + |W(\mathbf{r}_1,\mathbf{r}_2)|^2, \tag{A20}$$

$$\langle E(\mathbf{r}_1)E^*(\mathbf{r}_2)\rangle = W(\mathbf{r}_1,\mathbf{r}_2), \tag{A21}$$

$$\langle E^*(\mathbf{r}_1)E(\mathbf{r}_2)\rangle = W^*(\mathbf{r}_1,\mathbf{r}_2), \tag{A22}$$

$$E_r^{(1)*}(\mathbf{r}_1)E_r^{(2)}(\mathbf{r}_2) = \sqrt{I_r^{(1)}(\mathbf{r}_1)I_r^{(2)}(\mathbf{r}_2)}e^{-i\Delta\phi}, \tag{A23}$$

$$E_r^{(1)}(\mathbf{r}_1)E_r^{(2)*}(\mathbf{r}_2) = \sqrt{I_r^{(1)}(\mathbf{r}_1)I_r^{(2)}(\mathbf{r}_2)}e^{i\Delta\phi}. \tag{A24}$$

Thus, Eqs. (A3)–(A24) yield the result for $G_S^{(1,2)}(\mathbf{r}_1,\mathbf{r}_2)$ in Eq. (7) of the main text.

[1] L. Mandel and E. Wolf, *Optical Coherence and Quantum Optics* (Cambridge University, Cambridge, 1995).

[2] A. T. Friberg and T. Setälä, Electromagnetic theory of optical coherence (invited), J. Opt. Soc. Am. A **33**, 2431 (2016).

[3] L. Ma and S. A. Ponomarenko, Optical coherence gratings and lattices, Opt. Lett. **39**, 6656 (2014).

[4] L. Ma and S. A. Ponomarenko, Free-space propagation of optical coherence lattices and periodicity reciprocity, Opt. Express **23**, 1848 (2015).

[5] Y. Chen, S. A. Ponomarenko, and Y. Cai, Experimental generation of optical coherence lattices, Appl. Phys. Lett. **109**, 061107 (2016).

[6] Y. Chen, S. A. Ponomarenko, and Y. Cai, Self-steering partially coherent beams, Sci. Rep. **7**, 39957 (2017).

[7] H. Mao, Y. Chen, C. Liang, L. Chen, Y. Cai, and S. A. Ponomarenko, Self-steering partially coherent vector beams, Opt. Express **27**, 14353 (2019).

[8] S. A. Ponomarenko, Self-imaging of partially coherent light in graded-index media, Opt. Lett. **40**, 566 (2015).

[9] X. Liu, J. Yu, Y. Chen, Y. Cai, and S. A. Ponomarenko, Propagation of optical coherence lattices in the turbulent atmosphere, Opt. Lett. **41**, 4182 (2016).

[10] F. Wang, Y. Chen, L. Guo, L. Liu, and Y. Cai, Complex Gaussian representations of partially coherent beams with nonconventional degrees of coherence, J. Opt. Soc. Am. A **34**, 1824 (2017).

[11] S. A. Ponomarenko, Twisted Gaussian Schell-model solitons, Phys. Rev. E **64**, 036618 (2001).

[12] S. A. Ponomarenko and G. P. Agrawal, Asymmetric incoherent vector solitons, Phys. Rev. E **69**, 036604 (2004).

[13] E. Wolf, Significance and measurability of the phase of a spatially coherent optical field, Opt. Lett. **28**, 5 (2003).

[14] E. Wolf, Solution of the Phase Problem in the Theory of Structure Determination of Crystals from X-Ray Diffraction Experiments, Phys. Rev. Lett. **103**, 075501 (2009).

[15] A. Classen, K. Ayyer, H. N. Chapman, R. Röhlsberger, and J. von Zanthier, Incoherent Diffractive Imaging via Intensity Correlations of Hard X Rays, Phys. Rev. Lett. **119**, 053401 (2017).

[16] Y. K. Park, C. Depeursinge, and G. Popescu, Quantitative phase imaging in biomedicine, Nat. Photon. **12**, 578 (2018).

[17] M. I. Akhlaghi and A. Dogariu, Tracking hidden objects using stochastic probing, Optica **4**, 447 (2017).

[18] M. Batarseh, S. Sukhov, Z. Shen, H. Gemar, R. Reznavi, and A. Dogariu, Passive sensing around the corner using spatial coherence, Nat. Commun. **9**, 3629 (2018).

[19] R. Schneider *et al.*, Quantum imaging with incoherently scattered light from a free-electron laser, Nat. Phys. **14**, 126 (2018).

[20] A. Beckus, A. Tamasan, A. Dogariu, A. F. Abouraddy, and G. K. Atia, On the inverse problem of source reconstruction from coherence measurements, J. Opt. Soc. Am. A **35**, 959 (2018).

[21] K. Saastamoinen, L.-P. Leppänen, I. Vartiainen, A. T. Friberg, and T. Setälä, Spatial coherence of light measured by nanoscattering, Optica **5**, 67 (2018).

[22] H. Partanen, J. Turunen, and J. Tervo, Coherence measurement with digital micromirror device, Opt. Lett. **39**, 1034 (2014).

[23] H. Arimoto and Y. Ohtsuka, Measurements of the complex degree of spectral coherence by use of a wave-front-folded interferometer, Opt. Lett. **22**, 958 (1997).

[24] M. Santarsiero and R. Borghi, Measuring spatial coherence by using a reversed-wavefront Young interferometer, Opt. Lett. **31**, 861 (2006).

[25] R. R. Naraghi, H. Gemar, M. Batarseh, A. Beckus, G. Atia, S. Sukhov, and A. Dogariu, Wide-field interferometric measurement of a nonstationary complex coherence function, Opt. Lett. **42**, 4929 (2017).

[26] A. Bhattacharjee, S. Aarav, and A. K. Jha, Two-shot measurement of spatial coherence, Appl. Phys. Lett. **113**, 051102 (2018).
[27] M. Koivurova, H. Partanen, J. Lahyani, N. Cariou, and J. Turunen, Scanning wavefront folding interferometers, Opt. Express **27**, 7738 (2019).
[28] D. Kohler and L. Mandel, Operational approach to the phase problem of optical coherence, J. Opt. Soc. Am. A **60**, 280 (1970).
[29] D. Kohler and L. Mandel, Source reconstruction from the modulus of the correlation function: A practical approach to the phase problem of optical coherence theory, J. Opt. Soc. Am. A **63**, 126 (1973).
[30] Y. Shao, X. Lu, S. Konijnenberg, C. Zhao, Y. Cai, and H. P. Urbach, Spatial coherence measurement and partially coherent diffractive imaging using self-referencing holography, Opt. Express **26**, 4479 (2018).
[31] X. Lu, Y. Shao, C. Zhao, S. Konijnenberg, X. Zhu, Y. Tang, Y. Cai, and H. Urbach, Noniterative spatially partially coherent diffractive imaging using pinhole array mask, Adv. Photon. **1**, 016005 (2019).
[32] M. Takeda, W. Wang, D. N. Naik, and R. K. Singh, Spatial statistical optics and spatial correlation holography: A review, Opt. Rev. **21**, 849 (2014).
[33] J. K. Wood, K. A. Sharma, S. Cho, T. G. Brown, and M. A. Alonso, Using shadows to measure spatial coherence, Opt. Lett. **39**, 4927 (2014).
[34] K. A. Sharma, T. G. Brown, and M. A. Alonso, Phase-space approach to lensless measurements of optical field correlations, Opt. Express **24**, 16099 (2016).
[35] K. A. Sharma, G. Costello, E. Vélez-Juárez, T. G. Brown, and M. A. Alonso, Measuring vector field correlations using diffraction, Opt. Express **26**, 8301 (2018).
[36] J. W. Goodman, *Statistical Optics* (John Wiley & Sons, New York, 1985).
[37] T. Hassinen, J. Tervo, T. Setälä, and A. T. Friberg, Hanbury Brown–Twiss effect with electromagnetic waves, Opt. Express **19**, 15188 (2011).
[38] Y. Chen, F. Wang, L. Liu, C. Zhao, Y. Cai, and O. Korotkova, Generation and propagation of a partially coherent vector beam with special correlation functions, Phys. Rev. A **89**, 013801 (2014).
[39] T. Shirai, Modern aspects of intensity interferometry with classical light, Prog. Opt. **62**, 1 (2017).
[40] X. Liu, F. Wang, L. Liu, Y. Chen, Y. Cai, and S. A. Ponomarenko, Complex degree of coherence measurement for classical statistical fields, Opt. Lett. **42**, 77 (2017).
[41] F. Wang, X. Liu, Y. Yuan, and Y. Cai, Experimental generation of partially coherent beams with different complex degrees of coherence, Opt. Lett. **38**, 1814 (2013).
[42] M. W. Hyde IV, S. Bosu, D. G. Voelz, and X. Xiao, Experimentally generating any desired partially coherent Schell-model source using phase-only control, J. Appl. Phys. **118**, 093102 (2015).
[43] M. W. Hyde IV, S. Bose-Pillai, D. G. Voelz, and X. Xiao, Generation of Vector Partially Coherent Optical Sources Using Phase-Only Spatial Light Modulators, Phys. Rev. Appl. **6**, 064030 (2016).
[44] Y. Cai, Y. Chen, J. Yu, X. Liu, and L. Liu, Generation of partially coherent beams, Prog. Opt. **62**, 157 (2017).
[45] M. V. da Cunha Pereira, L. A. P. Filpi, and C. H. Monken, Cancellation of atmospheric turbulence effects in entangled two-photon beams, Phys. Rev. A **88**, 053836 (2013).
[46] A. J. Jesus-Silva, J. G. Silva, C. H. Monken, and E. J. S. Fonseca, Experimental cancellation of aberrations in intensity correlation in classical optics, Phys. Rev. A **97**, 013832 (2018).
[47] T. A. Smith and Y. Shih, Turbulence-Free Double Slit Interometer, Phys. Rev. Lett. **120**, 063606 (2018).
[48] X. Liu, F. Wang, C. Wei, and Y. Cai, Experimental study of turbulence-induced beam wander and deformation of a partially coherent beam, Opt. Lett. **39**, 3336 (2014).
[49] C. Bonato, A. V. Sergienko, B. E. A. Saleh, S. Bonora, and P. Villoresi, Even-Order Aberration Cancellation in Quantum Interferometry, Phys. Rev. Lett. **101**, 233603 (2008).
[50] O. Minaeva, C. Bonato, B. E. A. Saleh, D. S. Simon, and A. V. Sergienko, Odd- and Even-Order Dispersion Cancellation in Quantum Interferometry, Phys. Rev. Lett. **102**, 100504 (2009).
[51] V. Torres-Company, H. Lajunen, and A. T. Friberg, "Nonlocal" dispersion cancelation with classical light, New J. Phys. **11**, 063041 (2009).